



# Magnetization States of All-Oxide Spin Valves Controlled by Charge-orbital Ordering of Coupled Ferromagnets

SUBJECT AREAS:  
MAGNETIC PROPERTIES  
AND MATERIALS  
SPINTRONICS  
MAGNETIC DEVICES  
ELECTRONIC DEVICES

Han-Chun Wu<sup>1</sup>, Oleg N. Mryasov<sup>2</sup>, Mohamed Abid<sup>3,4</sup>, Kevin Radican<sup>1</sup> & Igor V. Shvets<sup>1</sup>

<sup>1</sup>CRANN, School of Physics, Trinity College, Dublin 2, Ireland, <sup>2</sup>Department of Physics and MINT, University of Alabama, Tuscaloosa, AL 35487, USA, <sup>3</sup>Ecole Polytechnique Federale de Lausanne/IPMC/LPMN, Station 3, CH 1015, Switzerland, <sup>4</sup>King Saud University, Riyadh 11451, Saudi Arabia.

Received  
16 January 2013

Accepted  
18 April 2013

Published  
13 May 2013

Correspondence and  
requests for materials  
should be addressed to  
H.-C.W. (wuhc@tcd.  
ie)

**Charge-orbital ordering is commonly present in complex transition metal oxides and offers interesting opportunities for novel electronic devices. In this work, we demonstrate for the first time that the magnetization states of the spin valve can be directly manipulated by charge-orbital ordering. We investigate the interlayer exchange coupling (IEC) between two epitaxial magnetite layers separated by a nonmagnetic epitaxial MgO dielectric. We find that the state of the charge-orbital ordering in magnetite defines the strength, and even the sign of the IEC. First-principles calculations further show that the charge-orbital ordering modifies the spin polarized electronic states at the Fe<sub>3</sub>O<sub>4</sub>/MgO interfaces and results in a sufficiently large phase shift of wave function which are responsible for the observed IEC sign change across Verwey temperature. Our findings may open new interesting avenues for the electric field control of the magnetization states of spin valves via charge-orbital ordering driven IEC sign change.**

Over the past five decades, the performance of electronic devices improved massively driven by the reduction in the size of transistors. It is increasingly clear that scientists need to develop novel mechanisms for the control of electron charge and spin degrees of freedom. An example of this could be based on the effect of spin torque due to spin polarized current. This mechanism involves the interaction of conduction-electron spins with localized moments leading an effectively voltage controlled spin valve magnetization states<sup>1–4</sup>. These results add new possibilities for realizing earlier proposed reconfigurable non-volatile logic elements utilizing, for instance, the magnetoresistance of two coupled magnetic layers with different coercive fields<sup>5</sup>. Finding suitable materials to effectively implement these ideas is one of main issues in this exciting field. Strongly correlated conducting oxides are an important class of materials in this mission<sup>6</sup>. These materials present a fascinating interplay between magnetic and electric properties, combined with charge-orbital ordering<sup>7</sup>. The importance of complex oxide systems for the development of novel device functions was emphasized in a recent study<sup>8</sup>. However, the study stopped short of reporting experimental work to substantiate the proposed device functionalities. One of most fascinating and invaluable oxides for revealing new physics and new phenomena involving spin, orbital and charge-orbital ordering is magnetite, Fe<sub>3</sub>O<sub>4</sub>. It is the archetype magnetic material with a narrow 3d band, and therefore strong-correlation effects are expected. Indeed, it shows complex charge and orbital ordering, and at Verwey temperature,  $T_V = 120$  K, the material undergoes a metal-insulator phase transition leading to a sharp drop in conductivity<sup>9</sup>. Recently electric field-induced switching between the low- and high-conductance states was found in magnetite<sup>10</sup>. On the other hand, one of the possible and perhaps least explored approaches for new functionalities of spin electronic devices is based on finding ways for the direct manipulation the interlayer exchange coupling (IEC). The discovery of the giant magnetoresistance and oscillatory IEC in fully metallic multilayer systems have enabled the development of new classes of spin valve based sensors and magnetic random access memories<sup>11,12</sup>. How to manipulate magnetization in these structures with nanoscale resolution is the key question<sup>13</sup>. The switching could also be implemented by means of multiferroic materials via a voltage switchable exchange bias<sup>14</sup> or take advantage of a ferroelectric as the barrier material where the magnetization could be switched by an applied electric field through the switching of the ferroelectric order parameter<sup>15–17</sup>.

In this work, we present both experimental and theoretical results that for the first time demonstrate that the magnetization states (parallel or anti-parallel) of the spin valve can be directly manipulated by charge-orbital ordering of the coupled magnetic electrodes. We investigate the IEC between two epitaxial magnetite layers



separated by a nonmagnetic epitaxial MgO dielectric. We show that the state of the charge-orbital ordering in magnetite defines the strength, and even the very sign of the IEC. The IEC sign switching appears at the exact temperature of the  $\text{Fe}_3\text{O}_4$  high-to-low conductance transition which changes the magnetization states of spin valve from an anti-parallel (parallel) to a parallel (anti-parallel) state. This opens new interesting avenues for the control of magnetization states of spin valve via the charge-orbital ordering in coupled ferromagnets.

## Results

Our experimental study is performed on fully epitaxial  $\text{Fe}_3\text{O}_4/\text{MgO}/\text{Fe}_3\text{O}_4/\text{NiO}/\text{MgO}(100)$  stacks. Stacks with different MgO spacer thickness were prepared on the same MgO substrate using a shadow mask inside the molecular beam epitaxy system (Fig. S1 in the Supplementary). The purpose of the NiO (15 nm) under-layer is

to enhance the coercivity of the bottom  $\text{Fe}_3\text{O}_4$  pinned layer with respect to the top  $\text{Fe}_3\text{O}_4$  free layer. The thickness of both  $\text{Fe}_3\text{O}_4$  layers was 10 nm and that of the MgO spacer was varied between 0.8 nm and 3 nm. Reflection high energy electron diffraction (RHEED) was employed to confirm the epitaxial growth and establish the growth mode. The presence of the RHEED intensity oscillations confirms that the films grew in a layer-by-layer mode with a growth rate of 0.3 Å/s for  $\text{Fe}_3\text{O}_4$  and 0.05 Å/s for MgO respectively<sup>18</sup>. Detailed RHEED characterization can be found in the Supplementary. One can see from Figs. S2c that MgO barrier layer was epitaxially grown on the  $\text{Fe}_3\text{O}_4/\text{NiO}$  bilayer and that the MgO barrier with a thickness of 0.8 nm (less than 4 monolayer) has the same quality as MgO substrate which indicate a sharp interface between MgO and bottom  $\text{Fe}_3\text{O}_4$  and also guaranteed a sharp interface between MgO and top  $\text{Fe}_3\text{O}_4$ . Fig. S3 and the red curve in Fig. 1e show magnetization versus temperature for a 10 nm thick  $\text{Fe}_3\text{O}_4$  and  $\text{Fe}_3\text{O}_4/\text{MgO}/\text{Fe}_3\text{O}_4/\text{NiO}$

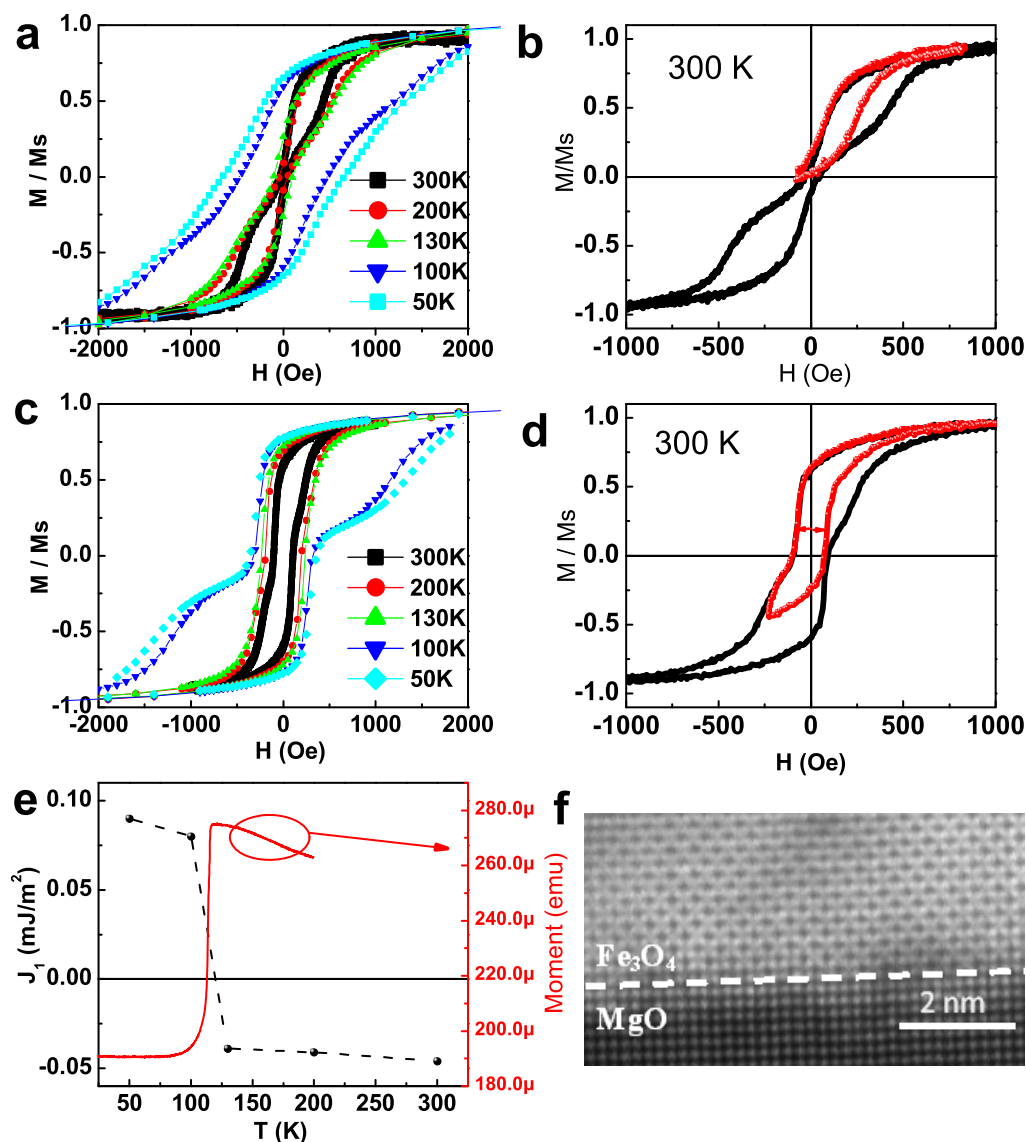


**Figure 1** | Temperature dependent magnetic hysteresis loops measured along [100] direction and calculated IEC  $J_1$  as a function of temperature. Magnetic hysteresis loops of  $\text{Fe}_3\text{O}_4/\text{MgO}/\text{Fe}_3\text{O}_4/\text{NiO}$  multilayers for different MgO thickness measured at 300 K (black line), 200 K (red line), 130 K (green line), 100 K (dark blue line), and 50 K (light blue line), respectively. The thickness of the MgO spacers are (a) 0.8 nm and (c) 3 nm respectively. Room temperature  $M(H)$  loops and the corresponding minor loops for samples with MgO thickness of (b) 0.8 nm and (d) 3 nm respectively. The in-plane magnetic field was applied along the [100] direction. (e) Calculated IEC  $J_1$  as a function of temperature for the sample with a 0.8 nm thick MgO spacer obtained from the experimental data and magnetization as a function of temperature during the warming cycle in the presence of a 200 Oe in-plane field (Red curve). (f) HAADF STEM image shows the sharp interfaces between  $\text{Fe}_3\text{O}_4$  and MgO, where the darker columns and brighter columns in  $\text{Fe}_3\text{O}_4$  correspond to  $\text{Fe}^{2+}$  and  $\text{Fe}^{3+}$  respectively.

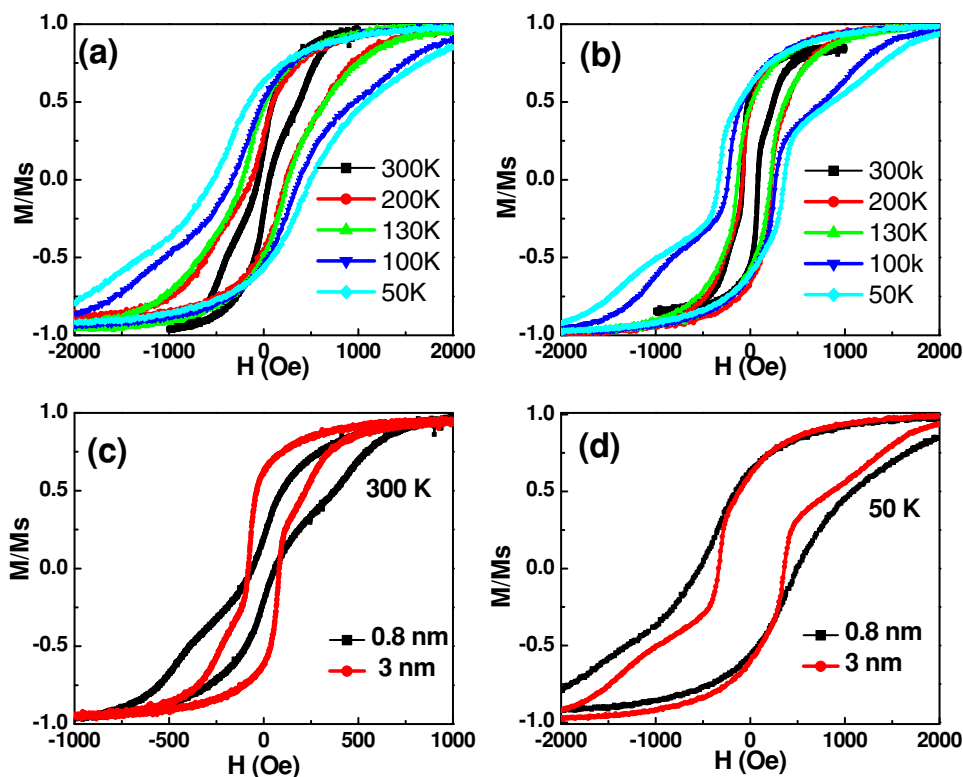


**Figure 2 | Temperature dependent magnetic hysteresis loops measured along [110] direction.** Magnetic hysteresis loops of  $\text{Fe}_3\text{O}_4/\text{MgO}/\text{Fe}_3\text{O}_4/\text{NiO}$  multilayers for different MgO thickness measured at different temperatures. The thickness of MgO spacers are (a) 0.8 nm and (b) 3 nm respectively. (c) and (d) are magnetic hysteresis loops of  $\text{Fe}_3\text{O}_4/\text{MgO}/\text{Fe}_3\text{O}_4/\text{NiO}$  multilayers for different MgO thickness measured at 300 K and 50 K. The in-plane magnetic field is applied along [110] direction.

with 0.8 nm thick MgO barrier layer during the heating cycle. The results shown in Fig. 1e and Fig. S3 confirm that the  $\text{Fe}_3\text{O}_4$  thin films undergo the Verwey transition at 115 K which is close to well established bulk values. To further demonstrate the quality of  $\text{Fe}_3\text{O}_4$  and the interface between the  $\text{Fe}_3\text{O}_4$  and MgO, Fig. S4 and Fig. 1f show the transmission electron microscopy (TEM) of  $\text{Fe}_3\text{O}_4/\text{MgO}/\text{Fe}_3\text{O}_4$  multilayer and the high angle angular dark field (HAADF) scanning transmission electron microscopy (STEM) image of the  $\text{Fe}_3\text{O}_4/\text{MgO}$  interface respectively. Sharp interfaces between MgO and  $\text{Fe}_3\text{O}_4$  layers are observed.

The magnetic properties of  $\text{Fe}_3\text{O}_4/\text{MgO}/\text{Fe}_3\text{O}_4/\text{NiO}$  stacks at different temperatures were examined by means of a Quantum Design Physical Properties Measurement System (PPMS). The in-plane magnetic field was applied along the [100] and [110] directions. Fig. 1c and Fig. S7b show the  $M(H)$  loops measured at different temperatures for the MgO layer thickness of 3 nm. At this large MgO thickness the exchange interaction between the two magnetite layers is very weak in comparison with magneto-static interactions. To confirm this, we show in Fig. 1d the minor loop. No shift was observed indicating that the top  $\text{Fe}_3\text{O}_4$  can rotate freely and no IEC is present between two  $\text{Fe}_3\text{O}_4$  layers. This makes the interpretation of the  $M(H)$  loops rather unambiguous. There are two characteristic field values,  $H_{c1}$  and  $H_{c2}$  which correspond to the coercivity of the layers of magnetite grown on the MgO and NiO respectively (See Fig. S8 in the Supplementary). The presence of the antiferromagnetic NiO layer increases the coercivity of the bottom magnetite layer due to the weak exchange bias effect which has been observed from both the  $M(H)$  measurements and planar hall effect measurements<sup>18</sup>. Fig. 1a shows the  $M(H)$  loops for the MgO thickness of 0.8 nm. Interestingly, above  $T_V$ , the difference between the  $H_{c1}$  and  $H_{c2}$  fields for a 0.8 nm thick MgO spacer is greater than that for a 3 nm MgO spacer. In particular, the moment at zero field is almost zero which

indicates a strong anti-ferromagnetic (AF) IEC between the two epitaxial  $\text{Fe}_3\text{O}_4$  layers. To demonstrate further the nature of the AF IEC and rule out possible domain effects, we show in Fig. 1b the  $M(H)$  minor loop. A large positive shift of 150 Oe was observed which indicates a strong AF IEC between two magnetite films. Remarkably, the shape of the  $M(H)$  loops changes drastically for a 0.8 nm thick MgO spacer just below  $T_V$ . At 50 K, one cannot distinguish clearly between  $H_{c1}$  and  $H_{c2}$ . For a quantitative interpretation of the measured  $M(H)$  loops, we use micromagnetic theory<sup>19,20</sup>. A more detailed description about the simulation can be found elsewhere<sup>19,20</sup>. These results are summarized in Fig. 1e showing that, above  $T_V$ , the two  $\text{Fe}_3\text{O}_4$  layers are AF exchange coupled through the MgO spacer and its IEC strength slightly decreases with decreasing temperature. At 300 K, a good fit is obtained with an IEC value of  $-4.6 \times 10^{-5}$  J/m<sup>2</sup> for the MgO spacer thickness of 0.8 nm and the fitting value compares well with the values reported by several groups<sup>21,22</sup>. Surprisingly, below  $T_V$ , the sign of the IEC changes from negative to positive. At 50 K, the IEC from fitting the  $M(H)$  loops is around  $1 \times 10^{-4}$  J/m<sup>2</sup> which is close to the value calculated directly using the formula in Ref. 23. The IEC sign switching appears at the exact temperature of the  $\text{Fe}_3\text{O}_4$  high-to-low conductance transition. A similar effect has been observed by applying the in-plane magnetic field along [110] direction (Fig. 2). Therefore, the change in the  $M(H)$  shape is due to the sign change of the IEC rather than any change in the in-plane magnetic anisotropy. To the best of our knowledge, our experimental results demonstrate for the first time that the IEC can be modulated by charge-orbital ordering of the coupled ferromagnetic electrodes. We would like to stress here the positive ferromagnetic (FM) IEC below  $T_V$  is not due to the orange peel coupling<sup>24</sup>. Firstly, orange peel coupling is due to a rough interface while sharp interfaces were verified with RHEED and HAADF STEM characterization. Secondly, we observe a large negative IEC

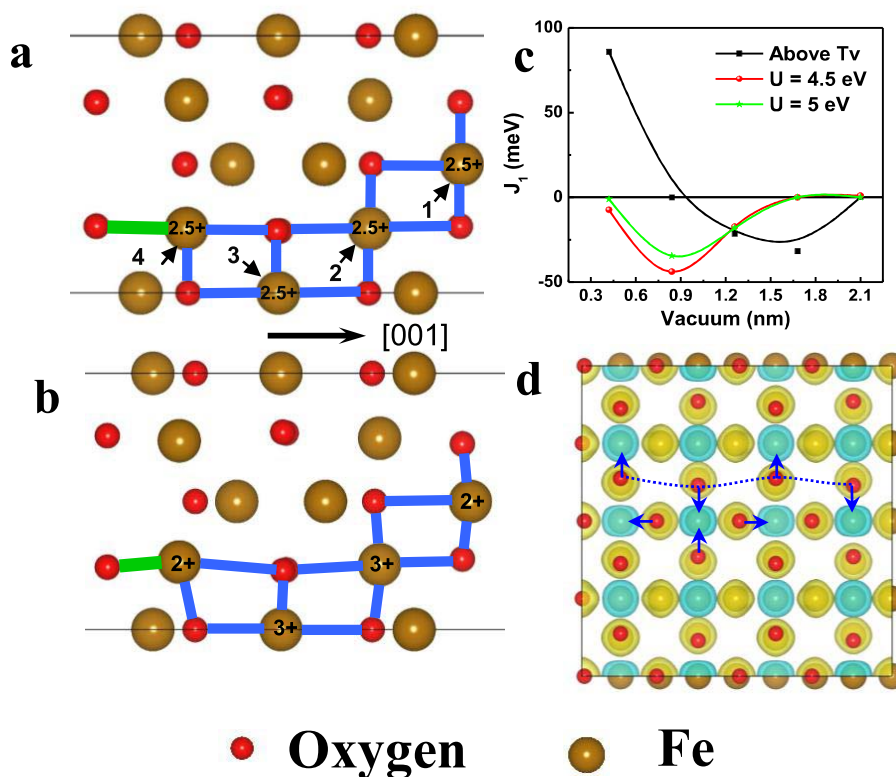


**Figure 3 | Calculated atomic structure.** Atomic structure and ionic charge distributions at (a)  $T > T_V$  and (b)  $T < T_V$ . Arrows [001] in Figs. (a) and (b) indicate the same direction perpendicular to the surface. (c) Calculated IEC  $J_1$  as a function of vacuum spacer thickness of  $\text{Fe}_3\text{O}_4/\text{vacuum}/\text{Fe}_3\text{O}_4$  at  $T > T_V$  (black line) and  $T < T_V$  for  $U = 4.5$  eV (red line) and  $U = 5$  eV (green line). (d) Atomic structure of (001) surface at  $T < T_V$ . The blue arrows indicate the apical O atoms move toward Fe atoms.

at room temperature while it is well established that the orange peel contribution has a positive sign. Thirdly, this sign change occurs very sharply at the Verwey transition temperature which is not expected for orange peel coupling.

It is well-known that local Coulomb interactions (between Fe 3d) and electron-lattice coupling play crucial roles in the  $\text{Fe}_3\text{O}_4$  Verwey transition both in the bulk and on the surface<sup>25–27</sup>. Recently, the charge ordering was found to be accompanied by structural distortion<sup>25</sup> and was described well by introducing the Coulomb on-site interaction  $U$  and the Hund's exchange  $J$  between B-site Fe 3d states using the LDA +  $U$  method<sup>26</sup>. The Vienna Ab Initio Simulation Package (VASP) implementation of the LDA +  $U$  method was used by Lodziana to investigate both the effects of local Coulomb correlation and electron-lattice coupling on the electronic states of the  $\text{Fe}_3\text{O}_4$  (001) surface<sup>27</sup>. In both cases of bulk and surface  $\text{Fe}_3\text{O}_4$ , model yields are consistent with experiment results. To summarize, above  $T_V$  basic electronic, magnetic, and structural properties of  $\text{Fe}_3\text{O}_4$  can be well explained by DFT-LDA while properties observed below  $T_V$  can be described within the LDA +  $U$  method with an effective Coulomb potential  $U$ . Below we use this model to gain an understanding of the role of charge-orbital ordering on IEC to interpret our observations. Fig. 3a shows the positions of some atoms of the unit cell used in the calculations, the atomic structure (Fig. 3b) was obtained through self-consistent total energy minimization for electronic and ionic degrees of freedom using the LDA +  $U$  method. The charge ordered pattern obtained from the calculations is similar to that proposed by Attfield *et al.*<sup>28</sup> and is also consistent with direct experimental observation<sup>29</sup>. The calculated charges ( $q$ ) and magnetic moments ( $M$ ) for B-site Fe atoms (the positions are marked in Fig. 3a) below  $T_V$  and above  $T_V$  are summarized in Table 1. From Table 1, one can clearly see that charge and orbital ordering indeed emerge self-consistently within the model used. The 3d orbital

average  $\delta q$  and average  $\delta M$  between  $\text{Fe}^{3+}$  and  $\text{Fe}^{2+}$  cations are 0.191  $e$  and 0.585  $\mu_B$  respectively, which are consistent with earlier reports<sup>26</sup>. The total charge difference between  $\text{Fe}^{2+}$  and  $\text{Fe}^{3+}$  ions ( $\delta q$  in Table 1) is mainly due to the  $t_{2g}$  d-orbital. In Fig. 3c we show the calculated IEC  $J_1$  as a function of vacuum spacer thickness of  $\text{Fe}_3\text{O}_4/\text{vacuum}/\text{Fe}_3\text{O}_4$  junctions below  $T_V$  ( $U = 4.5$  eV and  $U = 5.0$  eV) and above  $T_V$ . The vacuum spacer is chosen to represent a generic tunneling barrier. One can clearly see from Fig. 3c that the charge-orbital ordering changes the strength and even the sign of the long-range IEC. For  $\text{Fe}_3\text{O}_4/\text{vacuum}/\text{Fe}_3\text{O}_4$  junctions with a 4.2 nm thick vacuum spacer, the IEC is positive at  $T > T_V$  and changes to negative at  $T < T_V$  for  $U = 4.5$  eV. In Fig. 3b one can see that the charge and orbital ordering in  $\text{Fe}_3\text{O}_4$  leads to a complex lattice distortion. The Fe-O bonds formed by surface oxygen atoms with B-site Fe atoms (marked as green in Figs. 3a and 3b) have been dramatically modified due to charge-orbital ordering. The apical O atoms move toward the Fe atoms and result in Jahn-Teller deformations on the (001) surface below  $T_V$  (Fig. 3d). To further demonstrate the origin of the charge orbital ordering driven IEC sign change, we plotted in Fig. 4 the density of state (DOS) of the  $\text{Fe}_3\text{O}_4/\text{vacuum}$  (0.42 nm)/ $\text{Fe}_3\text{O}_4$  junction and the DOS of its surface oxygen atoms at  $T > T_V$  and  $T < T_V$  for  $U = 4.5$  eV. One can see that for junctions with a 0.42 nm vacuum spacer at  $T > T_V$ , when the magnetization of two  $\text{Fe}_3\text{O}_4$  layers changes from anti-parallel to parallel configuration, the total DOS of the junction and its surface oxygen shifts to the low energy state indicating a FM IEC. In contrast, at  $T < T_V$  for  $U = 4.5$  eV, when the magnetization of two  $\text{Fe}_3\text{O}_4$  layers changes from anti-parallel to parallel configuration, the total DOS of the junction and its surface oxygen shifts to the high energy state which means a AF IEC. We also plotted the spin density distribution in  $\text{Fe}_3\text{O}_4/\text{vacuum}$  (1.68 nm)/ $\text{Fe}_3\text{O}_4$  junctions for cases above  $T_V$  and below  $T_V$  in Figs. 4e and 4f respectively<sup>30</sup>. One can clearly see from Figs. 4e and





**Table 1** | Calculated charges ( $q$ ) and magnetic moments ( $M$ ) for B-site Fe atoms. Total and 3d orbital charges ( $q$ ) and magnetic moments ( $M$ ) for B-site Fe atoms (the positions are marked in Fig. 2a) calculated within the model prohibiting ( $T > T_V$ ) and allowing ( $T < T_V$ ) charge-orbital ordering. The vacuum thickness is 1.68 nm and  $U$  is set to be 4.5 eV

B-site Fe atom	$q$ (e)		$q_d$ (e)		$M$ ( $\mu_B$ )		$M_d$ ( $\mu_B$ )	
	$T > T_V$	$T < T_V$	$T > T_V$	$T < T_V$	$T > T_V$	$T < T_V$	$T > T_V$	$T < T_V$
Fe (1)	6.612	6.680	5.956	5.985	3.557	3.739	3.483	3.605
Fe (2)	6.789	6.761	5.987	5.856	3.573	4.126	3.551	4.086
Fe (3)	6.791	6.731	5.987	5.822	3.601	4.158	3.587	4.129
Fe (4)	6.744	7.057	5.946	6.074	3.161	3.446	3.149	3.439

4f that the changes in the electronic states at the interface modify the propagating wave functions in the barrier. Therefore, the origin of the charge ordering driven IEC sign change can be attributed to that the charge-orbital ordering modifies the surface states, particularly the spin polarization of surface oxygen atoms. The changes in the electronic states at the interface further result in a significantly large phase shift of the propagating wave functions in the barrier, which

defines the sign and strength of the IEC (See Fig. 3c and the following Fig. 5c).

## Discussion

The IEC sign change with temperature has been reported in metallic tri-layer systems<sup>31</sup> and the mechanism behind it is associated with a

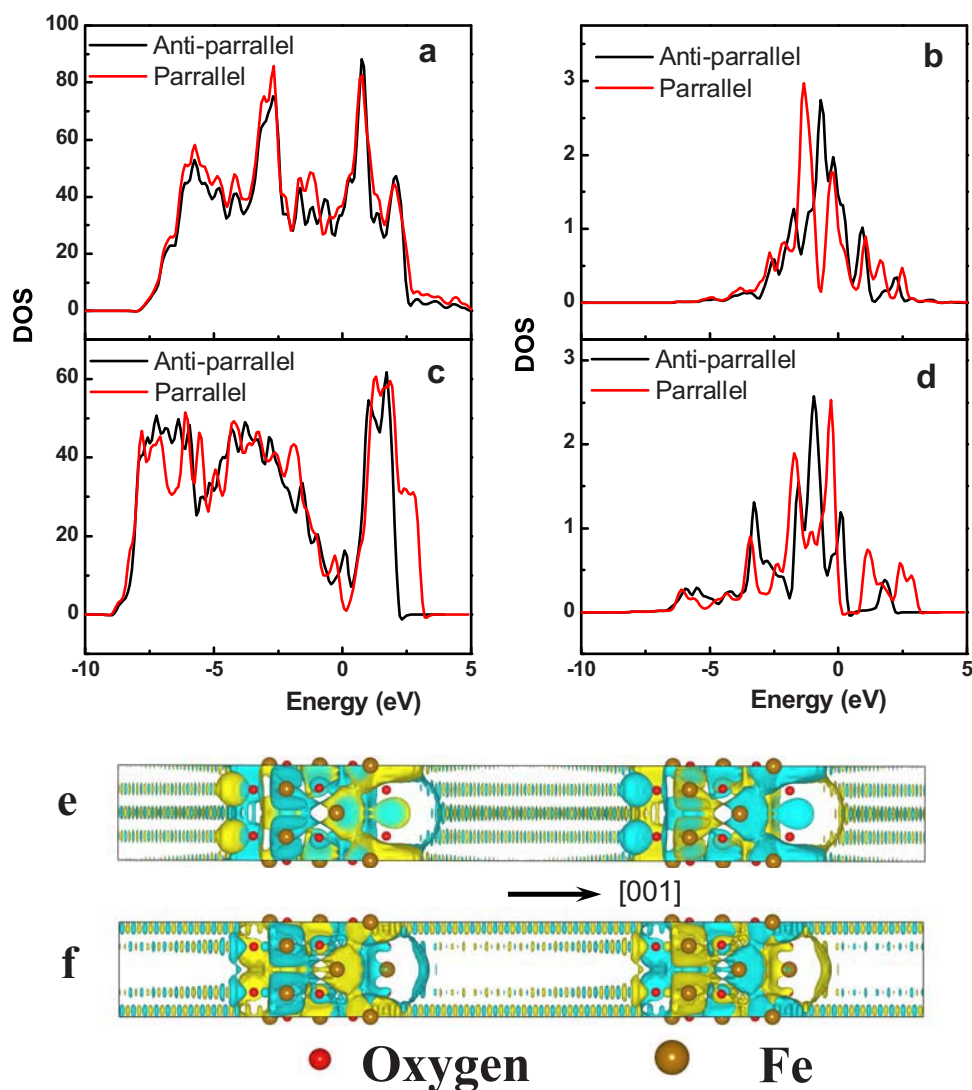


**Figure 4** | Calculated density of state and electron charge density distributions. DOS of the  $\text{Fe}_3\text{O}_4/\text{vacuum}$  (0.42 nm)/ $\text{Fe}_3\text{O}_4$  junction at  $T > T_V$  (a) and  $T < T_V$  for  $U = 4.5$  eV (c) and the DOS of its surface atoms at  $T > T_V$  (b) and  $T < T_V$  for  $U = 4.5$  eV (d). Calculated electron charge density distributions for spin up (blue) and spin down states (yellow) (e) without and (f) with CO. The spin density distributions are plotted for the sample with a vacuum thickness of 1.68 nm and the net magnetization of two  $\text{Fe}_3\text{O}_4$  layers are in the antiparallel configuration.

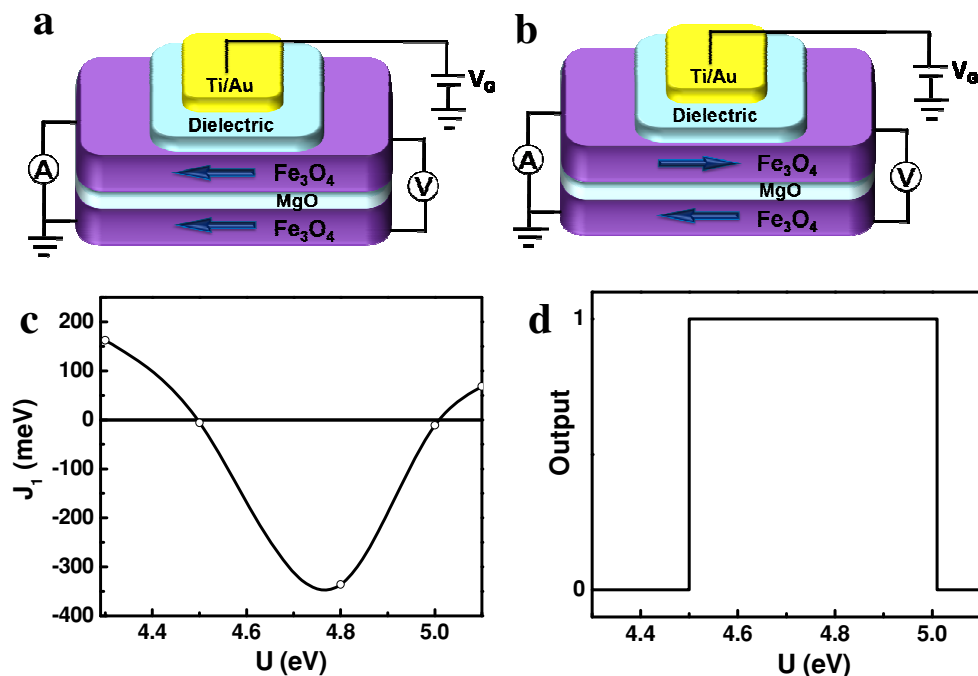


**Figure 5** | Conceptual illustration of MR element utilizing effect discovered in this study. Mutual orientation of two  $\text{Fe}_3\text{O}_4$  layers in magnetizations (a) parallel and (b) anti-parallel states controlled by the sign of IEC. This concept is further illustrated with calculated (c) IEC  $J_1$  and (d) logic output for generic  $\text{Fe}_3\text{O}_4/\text{vacuum}/\text{Fe}_3\text{O}_4$  junctions as a function of screened Coulomb interaction  $U$ .

slow functional dependence of the Ruderman-Kittel-Kasuya-Yosida (RKKY) IEC on temperature due to the Fermi distribution factor<sup>32</sup>. For  $\text{Fe}_3\text{O}_4$ , the IEC oscillating with spacer thickness has been reported in  $\text{TiN}/\text{Fe}_3\text{O}_4$  superlattices and it is attributed to the quantum confinement of the spin polarized electrons<sup>33</sup>. However, those mechanisms are entirely unsuitable for manipulating the magnetization state of spin valves at the nano-scale. In contrast, we report an abrupt change of IEC at the Verwey transition due to charge-orbital ordering of the magnetic electrodes. The mechanism put forward in this work is promising for voltage control of spin-valve magnetization state at the nano-scale since the charge-orbital ordering can be controlled by an electric field<sup>34</sup>. To highlight this, Figs. 5a and 5b show a schematic MR element where two  $\text{Fe}_3\text{O}_4$  layers are in magnetization parallel or anti-parallel states depending on the sign of the IEC. In the proposed MR element, the sign and strength of the IEC can be controlled by the top gate voltage ( $V_G$ ). For a FM IEC, without an external field, the magnetization of the two FM layers prefers a parallel configuration (Fig. 5a) and the resistance is relatively low (logic output 0). A spin valve with an AF IEC has high resistance (logic output 1) as the two FM layers are in an antiparallel magnetization state (Fig. 5b). Figs. 5c and 5d show the calculated IEC and logic output as a function of the screened Coulomb interaction  $U$  for  $\text{Fe}_3\text{O}_4/\text{vacuum}/\text{Fe}_3\text{O}_4$  junctions with a 4.2 nm thick vacuum spacer. This dependence represents changes in Coulomb correlations due to charge-orbital ordering tuned by  $V_G$ . One can see that the IEC oscillates as a function of  $U$ . For  $U = 4.3$  eV, the IEC is positive and the logic output is 0. Increasing  $U$  to 4.5 eV, the sign of the IEC changes from positive to negative and the corresponding logic output changes from 0 to 1. Further increasing  $U$  to 5.1 eV, the IEC becomes positive again.

In summary, we have experimentally and theoretically demonstrated that the magnetic exchange coupling of all oxide thin film layered stacks of (001)  $\text{NiO}/\text{Fe}_3\text{O}_4/\text{MgO}/\text{Fe}_3\text{O}_4$  can be manipulated by charge-orbital ordering in magnetic electrodes. We showed that the state of the charge orbital ordering in magnetite defines the strength, and even the very sign of the IEC. The IEC sign switching

appears at the exact temperature of the  $\text{Fe}_3\text{O}_4$  high-to-low conductance transition which changes the magnetization states of the spin valve from an anti-parallel (parallel) to a parallel (anti-parallel) state. This finding opens new possible ways for external stimuli (electrical field) control of magnetization states of spin valves via direct IEC manipulation by charge-orbital ordering. The mechanism of direct current driven magnetization switch and theoretically suggested IEC change due to the switching of ferroelectric polarization.

## Methods

**Sample preparation.** The  $\text{Fe}_3\text{O}_4/\text{MgO}/\text{Fe}_3\text{O}_4/\text{NiO}/\text{MgO}$  (100) stacks were grown on the same MgO (001) single crystal substrates using a shadow mask inside an oxygen plasma assisted molecular beam epitaxy system. The substrates were chemically cleaned prior to their insertion into the growth chamber and then cleaned in situ at 600°C in UHV for 1/2 hour followed by annealing in  $1 \times 10^{-5}$  Torr oxygen for 2 hours duration. The NiO epilayer (15 nm) was deposited at a substrate temperature of 600°C with an oxygen partial pressure  $5 \times 10^{-6}$  Torr. After the NiO growth, the sample was cooled to 250°C and a 10 nm  $\text{Fe}_3\text{O}_4$  film was grown which serves as the bottom FM layer<sup>18,19</sup>. Then a single crystalline MgO (001) was formed at 250°C with a rather low deposition rate 0.05 Å/s and annealed at 250°C for 20 min in a vacuum of  $5 \times 10^{-9}$  Torr. The thickness of MgO spacer is controlled by placing the shadow mask at different positions. Subsequently, a second (top)  $\text{Fe}_3\text{O}_4$  layer was deposited using the same growth conditions as those for the first  $\text{Fe}_3\text{O}_4$  layer.

**Magnetic and transport measurements.** The magnetic and transport properties of  $\text{Fe}_3\text{O}_4/\text{MgO}/\text{Fe}_3\text{O}_4/\text{NiO}$  spin valves at different temperatures were examined by means of a Quantum Design Physical Properties Measurement System (14 T, Quantum Design). The minor loops are taken after a positive saturation of the sample.

**Micromagnetic simulation.** The micromagnetic calculations were performed with OOMMF code<sup>20</sup>. The system we considered consists of two magnetic thin films with the same thickness but different coercive fields ( $H_{c1}$  and  $H_{c2}$ ).

**First-principles calculation.** For the LDA + U simulations in this work, we use  $J = 0.89$  eV and  $U$  was varied between 4.3 eV and 5.5 eV<sup>26</sup>. We employed the projected augmented plane wave method (PAW)<sup>35</sup>, implemented within VASP<sup>36</sup>. The valence configuration  $3d^7 4s^1$  for Fe and  $2s^2 2p^4$  for O were used. The generalized gradient approximation<sup>37</sup> is used for the exchange-correlation energy. A monkhorst-pack  $6 \times 6 \times 2$  k-point grid was applied to fully optimize the atomic configurations. To model the IEC above  $T_V$ , we consider  $\text{Fe}_3\text{O}_4$  without lattice distortion in accordance with the measured lattice structure as shown in Fig. 2a.



1. Baek, S. H. *et al.* Ferroelastic switching for nanoscale non-volatile magnetoelectric devices. *Nat. Mater.* **9**, 309 (2010).
2. Tulapurkar, A. A. *et al.* Spin-torque diode effect in magnetic tunnel junctions. *Nature* **438**, 339 (2005).
3. Krivorotov, I. N. *et al.* Time-domain measurements of nano magnet dynamics driven by spin-transfer torques. *Science* **307**, 228 (2005).
4. Sunkey, J. *et al.* Measurement of the spin-transfer-torque vector in magnetic tunnel junctions. *Nat. Phys.* **4**, 67 (2008).
5. Ney, A., Pampuch, C., Koch, R. & Ploog, K. H. Programmable computing with a single magnetoresistive element. *Nature* **425**, 485 (2003).
6. Dagotto, E. Complexity in Strongly Correlated Electronic Systems. *Science* **309**, 257 (2005).
7. Imada, M., Fujimori, A. & Tokura, Y. Metal-insulator transitions. *Rev. Mod. Phys.* **70**, 1039–1263 (1998).
8. Takagi, H. & Hwang, H. Y. An Emergent Change of Phase for Electronics. *Science* **327**, 1601 (2010).
9. Verwey, Electronic Conduction of Magnetite (Fe<sub>3</sub>O<sub>4</sub>) and its Transition Point at Low Temperatures. *Nature* **144**, 327 (1939).
10. Lee, S. *et al.* Electrically driven phase transition in magnetite nanostructures. *Nature Mater.* **7**, 130 (2008).
11. Parkin, S. S. P., More, N. & Roche, K. P. Oscillations in exchange coupling and magnetoresistance in metallic superlattice structures: Co/Ru, Co/Cr and Fe/Cr. *Phys. Rev. Lett.* **64**, 2304 (1990).
12. Parkin, S. S. P. *et al.* Giant tunneling magnetoresistance at room temperature with MgO (100) tunnel barriers. *Nature Mater.* **3**, 862 (2004).
13. Chappert, C., Fert, A. & Nguyenvan Dau, F. The emergence of spintronics in data storage. *Nature Mater.* **6**, 813 (2007).
14. Laukhin, V. *et al.* Electric-Field Control of Exchange Bias in Multiferroic Epitaxial Heterostructures. *Phys. Rev. Lett.* **97**, 227201 (2006).
15. Tsymbal, E. Y. & Kohlstedt, H. Tunneling Across a Ferroelectric. *Science* **313**, 181 (2006).
16. Chanthbouala, A. *et al.* Solid-state memories based on ferroelectric tunnel junctions. *Nat. Nano.* **7**, 101 (2012).
17. Yin, Y. W. *et al.* Enhanced tunnelling electroresistance effect due to a ferroelectrically induced phase transition at a magnetic complex oxide interface. *Nat. Mater.* doi:10.1038/nmat3564.
18. Wu, H. C. *et al.* Transversal magneto-resistance in epitaxial Fe<sub>3</sub>O<sub>4</sub> and Fe<sub>3</sub>O<sub>4</sub>/NiO exchange biased system. *Appl. Phys. Lett.* **101**, 052402 (2012).
19. Wu, H. C., Arora, S. K., Mryasov, O. N. & Shvets, I. V. Antiferromagnetic interlayer exchange coupling between Fe<sub>3</sub>O<sub>4</sub> layers across a nonmagnetic MgO dielectric layer. *Appl. Phys. Lett.* **92**, 182502 (2008).
20. Donahue, M. J. & Porter, D. G. OOMMF user's guide, version 1.2a. Technical Report NISTIR6376, National Institute of Standards and Technology, Gaithersburg, MD, 1999.
21. Faure-Vincent, J. *et al.* Interlayer Magnetic Coupling Interactions of Two Ferromagnetic Layers by Spin Polarized Tunneling. *Phys. Rev. Lett.* **89**, 107206 (2002).
22. Katayama, T. *et al.* Interlayer exchange coupling in Fe/MgO/Fe magnetic tunnel junctions. *Appl. Phys. Lett.* **89**, 112503 (2006).
23. vander Heijden, P. A. A. *et al.* Interlayer coupling between Fe<sub>3</sub>O<sub>4</sub> layers separated by an insulating nonmagnetic MgO layer. *Phys. Rev. B* **55**, 11569 (1997).
24. Schrag, B. D. *et al.* Néel “orange-peel” coupling in magnetic tunneling junction devices. *Appl. Phys. Lett.* **77**, 2373 (2000).
25. Wright, J. P., Attfield, J. P. & Radaelli, P. G. Long Range Charge Ordering in Magnetite Below the Verwey Transition. *Phys. Rev. Lett.* **87**, 266401 (2001).
26. Leonov, I., Yaresko, A. N., Antonov, V. N., Korotin, M. A. & Anisimov, V. I. Charge and Orbital Order in Fe<sub>3</sub>O<sub>4</sub>. *Phys. Rev. Lett.* **93**, 146404 (2004).
27. Lodziana, Z. Surface Verwey Transition in Magnetite. *Phys. Rev. Lett.* **99**, 206402 (2007).
28. Attfield, J. P. *et al.* Electrostatically driven charge-ordering in Fe<sub>2</sub>OBO<sub>3</sub>. *Nature* **396**, 655 (1998).
29. Shvets, I. V. *et al.* Long-range charge order on the Fe<sub>3</sub>O<sub>4</sub> (001) surface. *Phys. Rev. B* **70**, 155406 (2004).
30. Momma, K. & Izumi, F. VESTA: a three-dimensional visualization system for electronic and structural analysis. *J. Appl. Crystallogr.* **41**, 653 (2008).
31. Döbrich, K. M. *et al.* Temperature-Induced Reversal of Magnetic Interlayer Exchange Coupling. *Phys. Rev. Lett.* **100**, 227203 (2008).
32. Bruno, P. Theory of interlayer magnetic coupling. *Phys. Rev. B* **52**, 411 (1995).
33. Orozco, A. *et al.* Oscillatory Exchange Coupling and Giant Positive Magnetoresistance in TiN/Fe<sub>3</sub>O<sub>4</sub> Superlattices. *Phys. Rev. Lett.* **83**, 1680 (1999).
34. Wong, J. J. I., Swartz, A. G., Zheng, R. J., Han, W. & Kawakami, R. K. Electric Field Control of the Verwey Transition and Induced Magnetoelectric Effect in Magnetite. arXiv:1202.6460v1.
35. Payne, M. C., Teter, M. P., Allan, D. C., Arias, T. A. & Joannopoulos, J. D. Iterative minimization techniques for ab initio total-energy calculations: molecular dynamics and conjugate gradients. *Rev. Mod. Phys.* **64**, 1045 (1992).
36. Kresse, G. & Hafner, J. Ab initio molecular dynamics for liquid metals. *Phys. Rev. B* **47**, R558 (1993).
37. Wang, Y. & Perdew, J. P. Correlation hole of the spin-polarized electron gas, with exact small-wave-vector and high-density scaling. *Phys. Rev. B* **44**, 13298 (1991).

## Acknowledgements

We thank Dr. S.S.P. Parkin at IBM Almaden Research Center to read the draft and give valuable comments. This work was supported by Science Foundation of Ireland (SFI) under Contract No. 06/IN.1/I91, National Plan for Science and technology (Nos. NPST 1598-02 and NPST 1466-02) of King Abdulaziz City for Science and Technology, and STARnet (a Semiconductor Research Corporation program sponsored by MARCO and DARPA). H.C.W. is grateful to the SFI Short Term Travel fellowship support during his stay at PKU, M.A. thanks the financial support from Saudi Aramco (project No. 6600028398), and O. M. acknowledges CNMS User support by Oak Ridge National Laboratory Division of Scientific User facilities, U.S. Department of Energy. This work made use of computing facilities at the Trinity Centre for High Performance Computing, supported by SFI.

## Author contributions

H.C.W. carried out the measurements, theoretical modeling, and wrote the article. O.N.M. and K.R. contributed to the theoretical modeling. I.V.S. and M.A. gave scientific advice. All of the authors contributed to discussion, data analysis and reviewed the manuscript.

## Additional information

**Supplementary information** accompanies this paper at <http://www.nature.com/scientificreports>

**Competing financial interests:** The authors declare no competing financial interests.

**License:** This work is licensed under a Creative Commons Attribution-NonCommercial-NoDerivs 3.0 Unported License. To view a copy of this license, visit <http://creativecommons.org/licenses/by-nc-nd/3.0/>

**How to cite this article:** Wu, H., Mryasov, O.N., Abid, M., Radican, K. & Shvets, I.V. Magnetization States of All-Oxide Spin Valves Controlled by Charge-orbital Ordering of Coupled Ferromagnets. *Sci. Rep.* **3**, 1830; DOI:10.1038/srep01830 (2013).